Zhu *et al.*
Natural Products and Bioprospecting (2026) 16:1
https://doi.org/10.1007/s13659-025-00553-4

Natural Products and Bioprospecting

ORIGINAL ARTICLE

Open Access

First discovery of triterpenoids and sterols from *Cotinus coggygria* var. *cinereus* Engl. with anti-inflammatory and antibacterial activities

Yue-Tong Zhu[1], Ze-Rui Li[1], Ren-Hao Chen[1], Jin-Hao Li[1], Wei Wang[1], Yu-Qi Gao[2*], Chun-Huan Li[1*] and Jin-Ming Gao[1*]

Abstract

This study led to the isolation of 17 triterpenoids, including two lanostane-type (**1** and **2**), two dammarane-type (**3** and **7**), ten tirucallane-type (**4** and **8**–**16**), and three oleanane-type (**17**–**19**) triterpenoids, as well as nine sterols (**5**, **6**, and **20**–**26**) from *Cotinus coggygria* var. cinereus Engl, which were first discovered from the genus *Cotinus*. Among them, coggygrenoids A–D (**1**–**4**), coggygrerol A (**5**), and coggygrerol B (**6**) are undescribed compounds. Additionally, seven flavonoids (**27**–**33**) were also isolated from this plant. Compound **15** displayed inhibitory activities in LPS-induced RAW 264.7 cells with an IC_{50} value 6.81 ± 0.15 μM. Molecular docking demonstrated that **15** exhibited favorable affinity for NLRP3 and iNOS. In vitro and in vivo antibacterial evaluations indicated that coggygrnoid C (**3**) exhibited significant inhibitory activity against methicillin-resistant *Staphylococcus aureus* ATCC BAA-1717 (USA300), with An MIC of 8 μg/mL. Further mechanistic investigations demonstrated that **3** exerted antibacterial activity by compromising the integrity of the cell wall and membrane. Notably, the combination of **3** with ampicillin exhibited an additive antibacterial effect. In the *Galleria mellonella* infection model, compound **3** exhibited comparable activity to that of the positive control at 20 mg/kg. These findings suggest that triterpenoids of *C. coggygria* are potential antibacterial lead agents.

Keywords *Cotinus coggygria* var. *cinereus* Engl., Triterpenoids, Sterols, Anti-inflammatory activity, Antibacterial activity

*Correspondence:
Yu-Qi Gao
gyq1225@nwu.edu.cn
Chun-Huan Li
chunhuanli@nwsuaf.edu.cn
Jin-Ming Gao
jinminggao@nwsuaf.edu.cn

Springer

Graphical Abstract

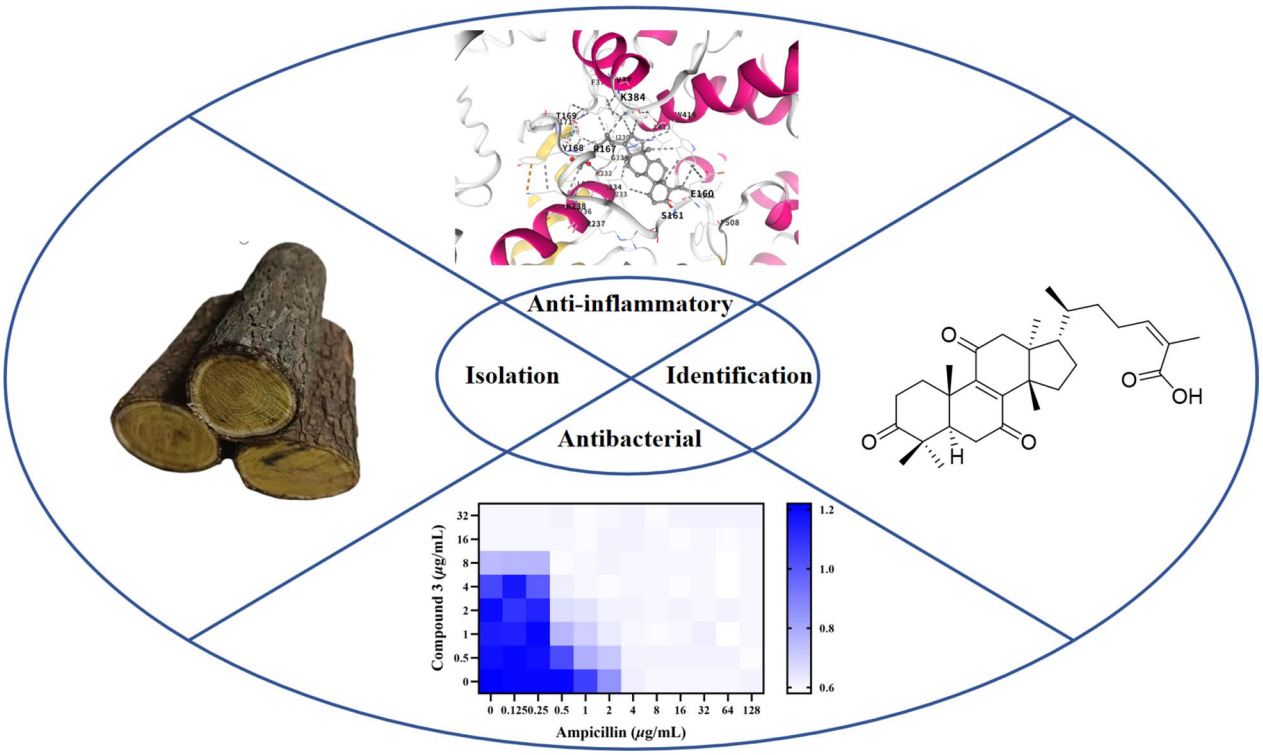

1 Introduction

Cotinus plants belong to the Anacardiaceae family and are categorized as deciduous shrubs or small trees [1]. These species are regarded as excellent ornamental tree species for landscaping purposes and served as pioneer tree species for afforestation on barren hills. *Cotinus* is rich in resources and widely distributed in Southern Europe, North America, China, and other regions. In China, *Cotinus* is primarily distributed in the mid-to-low altitude mountainous areas of Shaanxi, Shanxi, Henan, and Hebei provinces, with the main species being *Cotinus coggygria* var. *cinereus* Engl. [2]. *C. coggygria* contains a variety of chemical components, including flavonoids [3], gallic acid [4], and essential oils [5]. Historically, it has been extensively employed in traditional Chinese medicine and used for treating various diseases, including jaundice-type hepatitis, burns from fire or water, and lacquer dermatitis. Previous studies have shown that the extracts and chemical constituents of *C. coggygria* display extensive pharmacological effects, particularly in antioxidant [6, 7] hypotensive [8], liver damage repair [9], and antibacterial effects [10]. Triterpenoids are natural products composed of a basic nucleus consisting of six isoprene units totalling 30 carbon atoms, which have complex And diverse structures, encompassing over 100 different skeletal frameworks. A few of these are linear, monocyclic, bicyclic or tricyclic. The most common types are tetracyclic and pentacyclic triterpenes. Tetracyclic triterpenes are primarily classified as lanostane-, tirucallane-, dammarane- and cucurbitane-type. As important plant secondary metabolites, triterpenoids are involved in various physiological processes, such as oxidative stress, and exhibit pharmacological effects, including anti-inflammatory, neuroprotective, anti-Alzheimer's disease, antifungal and antitumour activities. As far as we know, no studies have been reported on the triterpenoids along with their biological activities in *C. coggygria*.

As part of an ongoing program of research into the identification of novel bioactive substances from traditional medicinal plants in the Tsinling Mountains [11–17], a phytochemical investigation was conducted on the tree stems and bark of *C. coggygria*. This investigation resulted in the isolation of a series of triterpenoids and sterols from the plant for the first time. The structures of the previously undescribed triterpenoids and sterols were elucidated using HRESIMS, NMR

Table 1 ^{1}H NMR (400 MHz) and ^{13}C NMR (100 MHz) data of **1**–**4** in $CDCl_3$

No	1		2		3		4	
	δ_H	δ_C	δ_H	δ_C	δ_H	δ_C	δ_H	δ_C
1	1.99 (m)	38.6	2.02 (m)	35.7	1.90 (m)	40.1	2.76 (m)	34.7
	1.44 (m)		1.62 (m)		1.42 (m)		1.50 (m)	
2	2.75 (m)	35.1	2.54 (m)	34.7	2.45 (m)	34.2	2.76 (m)	34.4
	2.25 (m)		2.46 (m)				2.42 (m)	
3		217.0		218.4		218.2		214.5
4		48.0		47.4		47.6		46.9
5	1.71 (m)	52.4	1.69 (m)	51.6	1.38 (m)	55.5	2.14 (m)	49.4
6	2.09 (m)	24.5	1.62 (m)	20.3	1.56 (m)	19.8	2.56 (m)	36.4
			1.46 (m)		1.46 (m)		2.47 (m)	
7	5.31 (m)	118.2	2.12 (m)	27.6	1.59 (m)	34.9		199.0
			1.96 (m)		1.36 (m)			
8		145.7		134.8		40.5		150.3
9	2.26 (m)	48.5		132.7	1.40 (m)	50.2		153.6
10		35.1		37.3		37.0		38.0
11	1.56 (m)	18.4	2.02 (m)	21.5	1.47 (m)	22.0		202.3
					1.17 (m)			
12	1.82 (m)	33.9	1.80 (m)	31.1	1.33 (m)	25.2	2.68 (d, 16.4)	51.3
	1.63 (m)		1.65 (m)		1.08 (m)		2.49 (d, 16.4)	
13		43.6		44.2	2.06 (m)	46.4		45.2
14		51.4		49.7		50.4		48.0
15	1.49 (m)	34.0	1.53 (m)	29.8	1.94 (m)	32.2	2.17 (m)	32.0
			1.25 (m)		1.22 (m)		1.69 (m)	
16	1.96 (m)	28.6	1.93 (m)	28.3	1.86 (m)	27.6	2.05 (m)	28.0
	1.30 (m)		1.32 (m)		1.76 (m)		1.38 (m)	
17	1.51 (m)	53.3	1.56 (m)	50.3	2.86 (m)	37.9	1.66 (m)	49.2
18	0.81 (s)	22.4	0.76 (s)	15.9	0.92 (s)	15.4	0.92 (s)	18.3
19	1.00 (s)	12.9	1.05 (s)	19.9	1.05 (s)	15.3	1.50 (s)	17.4
20	1.45 (m)	36.0	1.52 (m)	36.0		144.6	1.42 (m)	36.1
21	0.90 (d, 6.1)	18.6	0.90 (d, 6.5)	18.9	9.39 (s)	195.5	0.90 (d, 6.6)	18.2
22	1.74 (m)	33.7	1.76 (m)	33.9	6.77 (d, 13.9)	149.9	1.55 (m)	35.5
	1.18 (m)		1.30 (m)				1.16 (m)	
23	2.41 (m)	26.6	2.38 (m)	26.0	6.77 (q, 13.9)	121.8	2.57 (m)	26.8
	2.26 (m)		2.27 (m)				2.45 (m)	
24	6.49 (t, 7.4)	155.4	6.49 (t, 7.2)	155.6	6.30 (d, 13.9)	150.9	6.07 (t, 7.1)	146.8
25		139.2		139.2		71.3		126.2
26	1.75 (s)	9.2	1.75 (s)	9.4	1.40 (s)	29.8		172.4
27	9.39 (s)	195.5	9.39 (s)	195.6	1.40 (s)	29.8	1.92 (s)	20.7
28	1.04 (s)	24.7	1.09 (s)	26.0	1.08 (s)	26.9	1.13 (s)	25.5
29	1.11 (s)	21.7	1.05 (s)	21.2	1.04 (s)	21.1	1.15 (s)	21.4
30	1.02 (s)	27.6	0.90 (s)	24.4	0.92 (s)	16.2	1.10 (s)	24.1

spectroscopy, and electronic circular dichroism (ECD) calculations. Furthermore, all isolates were evaluated for their anti-inflammatory activity in lipopolysaccharide (LPS) stimulated nitric oxide (NO) production in RAW 264.7 cells and their antibacterial activity against five gram-positive and five gram-negative bacteria. Herein, we describe the isolation, structural elucidation, biological activities, and mechanism of action of the isolated triterpenoids and sterols.

2 Results and discussion

2.1 Structure elucidation

Coggygrnoid A (**1**) was obtained as a colorless solid with the molecular formula $C_{30}H_{46}O_2$, as established by a $[M+Na]^+$ ion peak at *m/z* 461.3382 in its HRESIMS spectrum (calcd for $C_{30}H_{46}O_2Na$, 461.3390), implying 11 degrees of unsaturation. The ^1H NMR data (Table 1) of **1** indicated the presence of one aldehyde proton [δ_H 9.39 (1H, s, H-27)] and two olefinic protons [δ_H 6.49 (1H, t, J=7.4 Hz, H-24), 5.31 (1H, m, H-7)]. In the high field, six tertiary methyl groups [δ_H 1.75 (3H, s, H_3-26), 1.11 (3H, s, H_3-29), 1.04 (3H, s, H_3-28), 1.02 (3H, s, H_3-30), 1.00 (3H, s, H_3-19), 0.81 (3H, s, H_3-18)], and a secondary methyl group [0.91 (3H, d, J=6.1 Hz, H_3-21)] were detected. The ^{13}C NMR and HSQC spectra of **1** (Table 1) showed thirty carbon signals sorted as one keto-carbonyl [δ_C 217.0 (C-3)], one aldehyde [δ_C 195.5 (C-27)], two double bonds [δ_C 118.2 (C-7), 145.7 (C-8), 155.4 (C-24), 139.2 (C-25)], four quaternary carbons [δ_C 48.0 (C-4), 35.1 (C-10), 43.6 (C-13), 51.4 (C-14)], four methines [δ_C 52.4 (C-5), 48.5 (C-9), 53.3 (C-17), 36.0 (C-20)], nine methylenes [δ_C 38.6 (C-1), 35.1 (C-2), 24.5 (C-6), 18.4 (C-11), 33.9 (C-12), 34.0 (C-15), 28.6 (C-16), 33.7 (C-22), 26.6 (C-23)], and seven methyls [δ_C 22.4 (C-18), 12.9 (C-19), 18.6 (C-21), 9.2 (C-26), 24.7 (C-28), 21.7 (C-29), 27.6 (C-30)]. Analysis of the above spectral data suggests that compound **1** is a lanostane triterpenoid with an *α*,*β*-unsaturated aldehyde structural fragment at the end of its side chain [18]. Further Analysis of the 2D NMR data of compound **1** led to the determination of its planar structure. The ^1H-^1H COSY correlations (Fig. 2) revealed the presence of four spin-coupling systems (H_2-1/H_2-2; H-5/H_2-6/H-7; H-5/H_2-11/H_2-12; H_2-15/H_2-16/H-17/H-20/(H_3-21)/H_2-22/H_2-23/H-24) in **1**. The HMBC correlations (Fig. 2) of H_3-28/H_3-29 with C-3, C-4, and C-5; H_3-19 with C-1, C-9, and C-10; H-2 with C-3; H-6 with C-8; H_3-18 with C-12, C-13, and C-17; H_3-30 with C-8, C-14, and C-15; and H_3-26 with C-24, C-25, and C-27 established the carbon connectivity of **1**, and the planar structure of compound **1** was then determined as (24*E*)-3-oxo-5*α*-lanosta-7,24-dien-27-al. The relative configuration of compound 1 was established by analysing its NOESY spectrum. The NOESY correlations (Fig. 3) observed between H_3-19 and H_3-18/H_3-28, as well as between H_3-18 and H-17 indicate a co-facial configuration, and assigned as *β*-orientation. Meanwhile, the NOESY correlations between H-5 and H-9/H_3-29/H_3-30 revealed that they were *α*-oriented. The double bond $\Delta^{24,25}$ was determined as *Z*-configuration by the NOE-correlation of CHO-27 with H-24. To confirm the absolute structure of **1**, experimental and calculated ECD spectra (Fig. 4) were obtained, which verified the structure of **1**, as shown in Fig. 1.

Coggygrnoid B (**2**) possessed a molecular formula of $C_{30}H_{46}O_2$ (eight degrees of unsaturation), as determined by the quasi-molecular ion peak 461.3395 $[M+Na]^+$ (calcd for $C_{30}H_{46}O_2Na$, 461.3390) in its HRESIMS spectrum. The characteristic signals of one aldehyde proton at δ_H 9.39 (1H, s, H-27), an olefinic proton at δ_H 6.49 (1H, t, J=7.2 Hz, H-24), and seven methyl signals at δ_H 1.75 (3H, s, H_3-26), 1.09 (3H, s, H_3-28), 1.05 (3H, s, H_3-29), 1.05 (3H, s, H_3-19), 0.90 (3H, d, J=6.5 Hz, H_3-21), 0.90 (3H, s, H_3-30), And 0.76 (3H, s, H_3-18) were presented in the ^1H NMR spectrum (Table 1). A total of 30 carbon resonances were well resolved in the ^{13}C NMR spectrum (Table 1), which were ascribed to seven methyls, ten methylenes, five methines (including two sp2 carbons), and eight quaternary carbons (one of which was carbonyl). Furthermore, a comparison of the ^1H and ^{13}C NMR data of **2** with those of compound **1** revealed close similarities. The Major difference was that the double bond at Δ 7(8) in **1** appeared at Δ 8(9) in **2**, which was supported by the chemical shifts of C-8 (δ_C 134.8), and C-9 (δ_C 132.7) and key HMBC correlations (Fig. 2) from H_2-7 to C-8 and from H_2-11 to C-9. Based on the biosynthetic relationship, combined with the NOESY correlations (Fig. 3) of H_3-18/H-17, H_3-18/H_3-19, H_3-19/H_3-28, H_3-29/H-5, H_3-30/H-5, and CHO-27/H-24, the absolute configuration of **2** was assigned to be the same as those of **1**. Although we did not obtain the CD curve of **2**, its specific optical rotation value, which was similar to that of **1**, also confirmed this assignment. Thus, the structure of compound **2** was elucidated as (24*E*)-3-oxo-5*α*-lanosta-8,24-dien-27-al.

Coggygrnoid C (**3**) was obtained as a faint yellowish gum and showed the molecular formula $C_{30}H_{46}O_3$ based on the HRESIMS ion at *m/z* 477.3330 $[M+Na]^+$ (calcd for $C_{30}H_{46}O_3Na$, 477.3339). The ^{13}C NMR and HSQC spectra (Table 1) showed 30 carbon resonances, which were classified as seven quaternary carbons (one ketone carbonyl and one olefinic), eight methines (one aldehyde and three olefinic), eight methylenes, and seven methyls by their chemical shifts and hybridization states. Combining the above data with the unsaturation of compound **3** indicates that it contains four rings in its structure. Additionally, the presence of one conjugated diene group [δ_H 6.77 (1H, d, J=13.9 Hz, H-22), 6.77 (1H, q, J=13.9 Hz, H-23), 6.30 (1H, d, J=13.9 Hz, H-24)], and seven tertiary methyls [δ_H 1.40 (3H, s, H_3-26), 1.40 (3H, s, H_3-27), 1.08 (3H, s, H_3-28), 1.05 (3H, s, H_3-19), 1.04 (3H, s, H_3-29), 0.92 (3H, s, H_3-18), And 0.92 (3H, s, H_3-30)] were evident from the ^1H NMR data (Table 1). The above data indicated that compound **3** was based on a dammarane triterpenoid skeleton similar to that of aglaiabbreviatin E (**7**) [19], with the main difference being the structure of the side chains. The exact structure of **3**

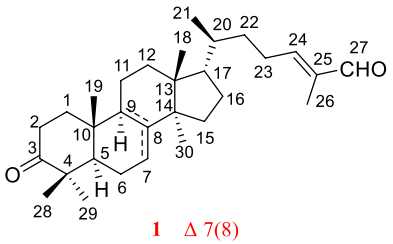

1 Δ 7(8)
2 Δ 8(9)

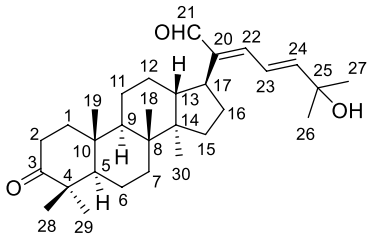

3

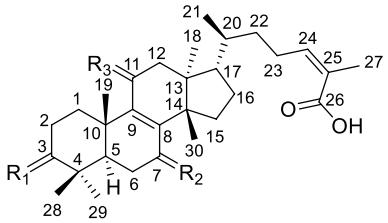

	R_1	R_2	R_3
4	O	O	O
8	O	O	H_2
9	α-OH, β-H	O	H_2
10	α-OH, β-H	O	O
11	O	H_2	H_2
12	α-H, β-OH	H_2	H_2

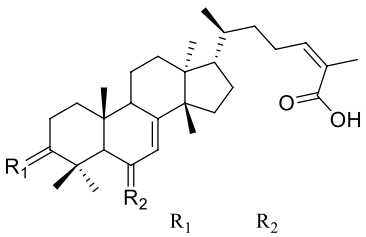

	R_1	R_2
13	O	O
14	α-OH, β-H	O
15	O	H_2
16	α-OH, β-H	H_2

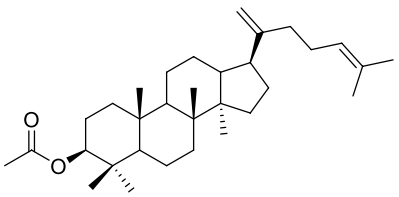

7

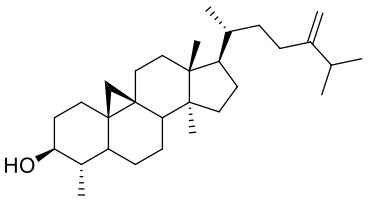

20

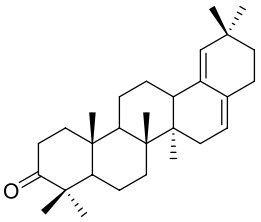

17

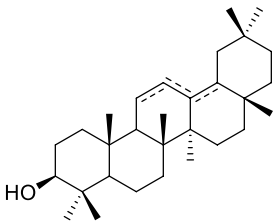

18 Δ 11(12) Δ 13(18)
19 Δ 12(13)

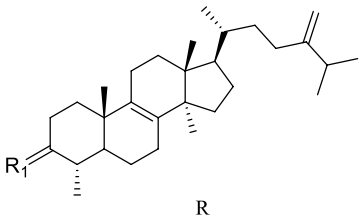

	R
21	O
22	α-H, β-OH

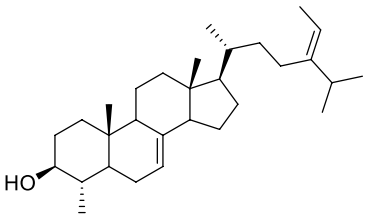

23

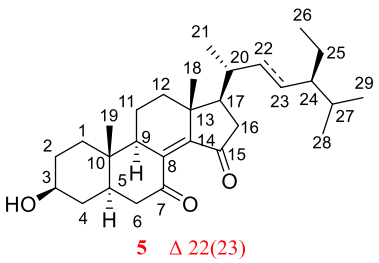

5 Δ 22(23)
6 – – –

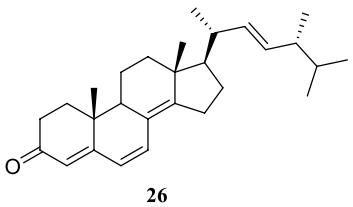

26

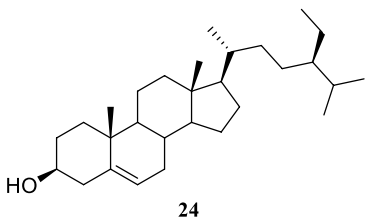

24

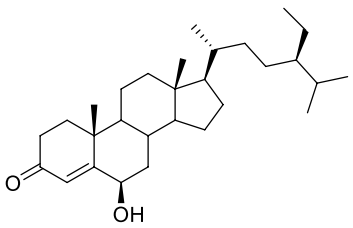

25

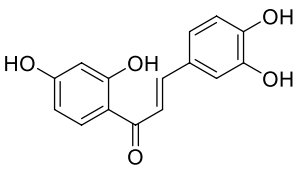

27

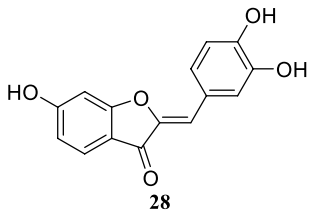

28

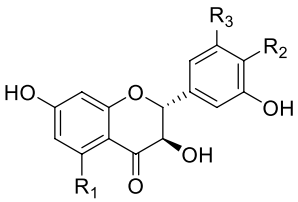

	R_1	R_2	R_3
29	OH	H	OH
30	H	OH	H

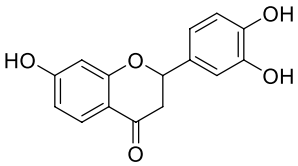

31 2*S*
32 2*R*

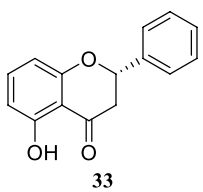

33

Fig. 1 Structures of compounds **1**–**33**

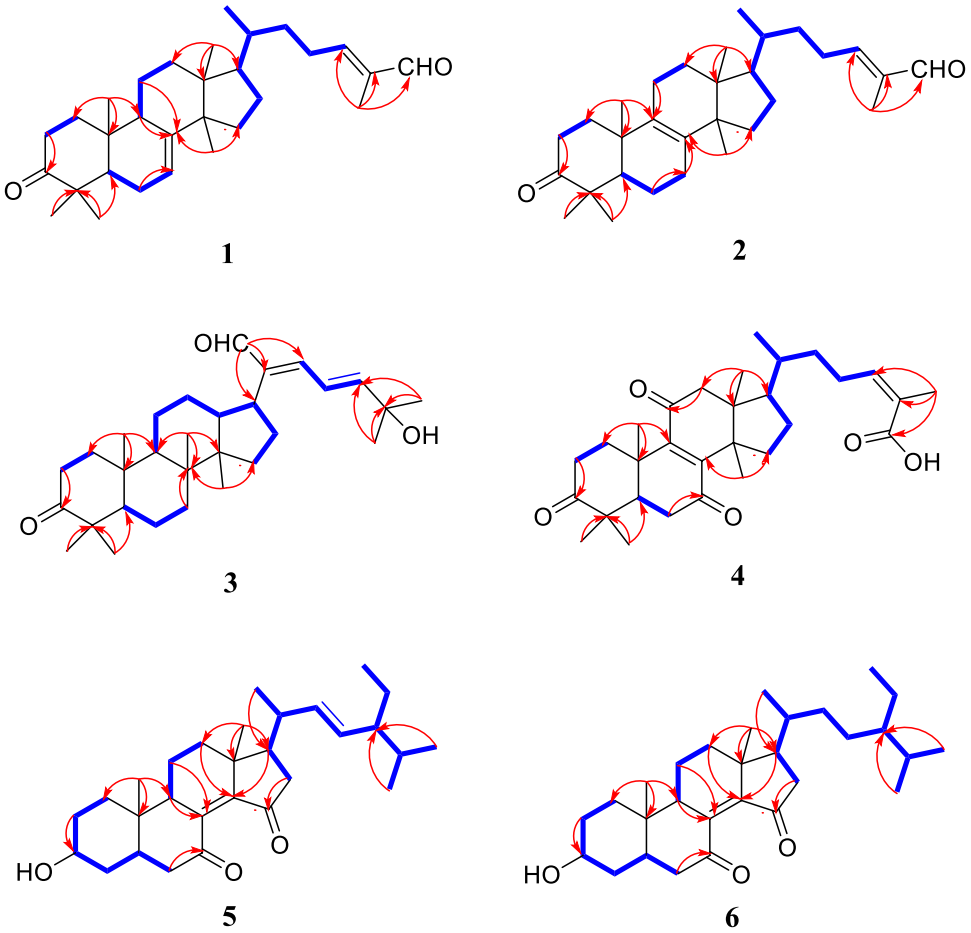

Fig. 2 Key HMBC and ^{1}H-^{1}H COSY correlations of compounds **1**–**6**

was deduced from the ^{1}H-^{1}H COSY and HMBC spectra (Fig. 2). The HMBC correlations arising from CHO-21 to C-17, C-20, and C-22; the gem-dimethyl protons (H_3-26 and H_3-27) to C-24, and C-25, and the spin system (H-22/H-23/H-24) indicated the presence of an *α*,*β*,*γ*,*δ*,-unsaturated aldehyde, which is consistent with the UV absorption curve. Compound **3** shared the same relative configuration as those of other dammarane-type triterpenoids. The NOESY correlations (Fig. 3) of H_3-18/H-13, H_3-18/H_3-19, and H_3-19/H_3-28 indicated co-facial orientation, which was assigned as *β*. Also, the NOESY correlations (Fig. 3) of H_3-29/H-5, H-9/H-5, H-9/H_3-30, and H_3-30/H-17 suggested that these were *α*-oriented. Therefore, the structure of compound **3** was elucidated as (21*E*,23*E*)-3-oxo-25-hydroxydammar-21-al-20,23-diene.

Coggygrnoid D (**4**) gave a molecular formula of $C_{30}H_{42}O_5$ as determined by an HRESIMS $[M-H]^-$ peak at 481.2957 (calcd for $C_{30}H_{41}O_5$, 481.2959). The ^{1}H NMR spectrum (Table 1) exhibited the presence of seven methyl signals, including one methyl doublet at δ_H 0.90 (d, J=6.6 Hz), five tertiary methyls, and one singlet methyl at δ_H 1.92. In addition, one olefinic proton was observed at δ_H 6.07 (t, J=7.1 Hz). The ^{13}C NMR spectrum (Table 1) displayed 30 carbon resonances. These were classified by HSQC experiment as three ketone carbonyls, one carboxyl group, two double bonds, four sp^3 quaternary carbons, three sp^3 methines, eight sp^3 methylenes, and seven methyls in the structure. Comparing the NMR data of **4** with 3,7-dioxo-8,24*Z*-tirucalladien-26-oic acid (**8**) revealed that the structures were closely related. The only difference was the presence of an additional carbonyl group at C-11 (δ_C 202.3). The two methylene proton resonances at δ_H 2.68 And 2.49, which exhibit larger coupling constant (J=16.4 Hz) and an HMBC correlation with δ_C 202.3 And 153.6 (Fig. 2), may be assigned to H_2-12 in the *α*-position relative to one of the carbonyl groups (δ_C 202.3). Moreover, the large downfield chemical shift at C-8 (δ_C 150.3) and upfield chemical shift at C-9 (δ_C 153.6) also confirmed that the olefinic bond was assigned between C-7 carbonyl and C-11carbonyl in **4**. The relative configuration of compound **4** was determined by the following correlation signals on the NOESY

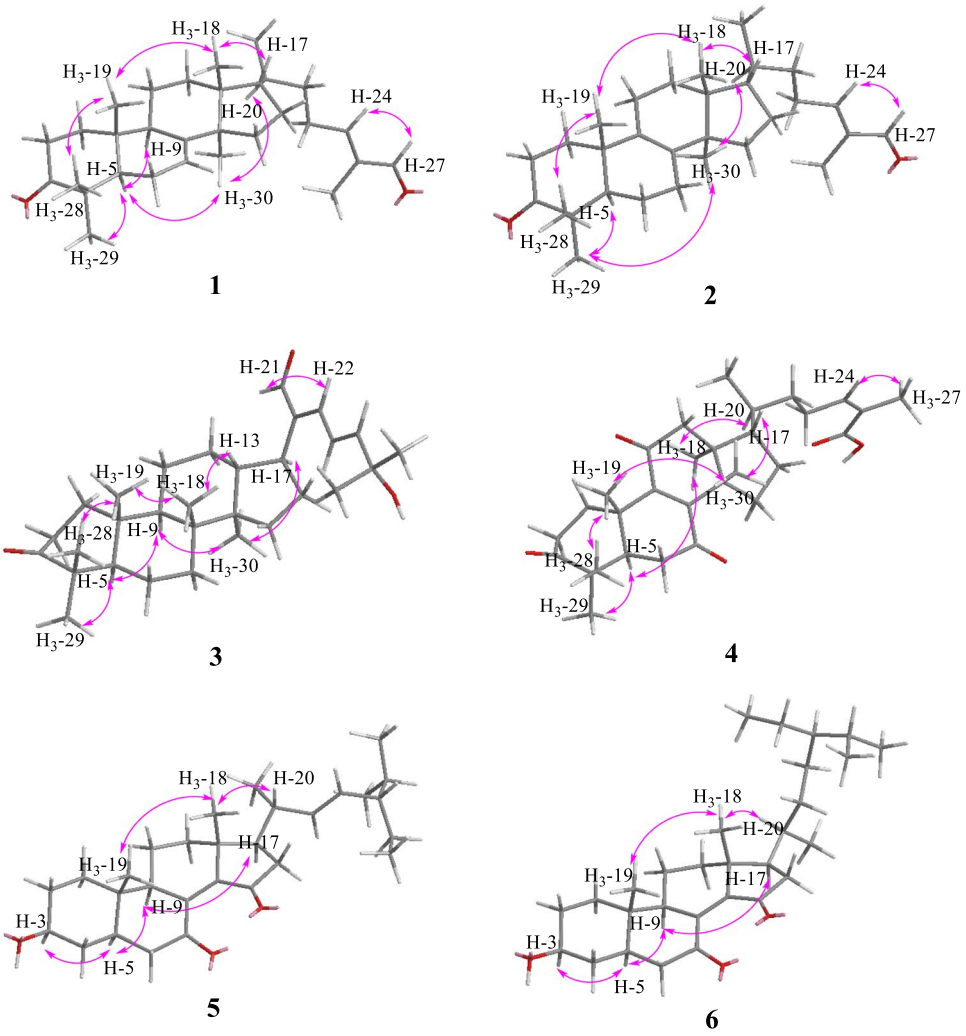

Fig. 3 Key NOESY correlations of compounds **1**–**6**

spectrum: H_3-19 and H_3-28, H_3-30; H_3-30 and H-7; H-5 and H_3-18, H_3-29; H-20 and H_3-18; H-24 and H_3-27. The high match of the experimental and calculated ECD spectra showed that the absolute configurations of **4** were 5*R*,10*S*,13*S*,14*S*,17*S*,20*S* (Fig. 4). Thus, the structure of **4** was confirmed as 3,7,11-trioxo-8,24*Z*-tirucalladien-26-oic acid.

Coggygrerol A (**5**) was a yellowish gum. The molecular formula of **5** was deduced from the quasi-molecular ion peak $[M+Na]^+$ at *m/z* 463.3179 (calcd for $C_{29}H_{44}O_3Na$, 463.3183) in the HRESIMS spectrum. The ^1H and ^{13}C NMR data (Table 2) indicated the presence of two ketone carbonyls [δ_C 202.1 (C-7), 205.1 (C-15)], two double bonds [δ_C 143.0 (C-8), 148.4 (C-14), 136.2 (C-22), 131.6 (C-23); δ_H 5.14 (1H, m, H-22), 5.14 (1H, m, H-23)], one oxygenated methine [δ_C 70.5 (C-3); δ_H 3.65 (1H, m, H-3)], and six methyl group [δ_C 18.2 (C-18), 12.5 (C-19), 21.7 (C-21), 12.4 (C-26), 21.2 (C-28), 19.3 (C-29); δ_H 1.01 (3H, s, H_3-18), 0.95 (3H, s, H_3-19), 1.10 (3H, d, J=7.2 Hz, H_3-21), 0.79 (3H, d, J=6.9 Hz, H_3-26), 0.83 (3H, d, J=6.4 Hz, H_3-28), 0.79 (3H, d, J=6.4 Hz, H_3-29)]. The ^1H and ^{13}C NMR spectra of compound **5** (Table 2) exhibited a high degree of similarity to those of the previously reported compound (3*S*,8*E*,22*E*)-hydroxystigmast-8,22-diene-7,11-dione [20] and as a typical steroidal skeleton. According to the subsequent comprehensive comparison of the data obtained for the two compounds, the bi-conjugate with a trans double bond (C-8, C-9) and two ketone carbonyl groups (C-7, C-11) in (3*S*,8*E*,22*E*)-hydroxystigmast-8,22-diene-7,11-dione was assumed to have transformed to $\Delta^{8,14}$ (double bond) and C-7/C-15 (two ketone carbonyl groups) in **5**. This assumption was confirmed by the HMBC correlations from H_2-6 to C-7; H-9, H_2-11 to C-8; H_2-12, H-17 to C-14; and those from H_2-16 to C-15 (Fig. 2). The configuration of the $\Delta^{2,3}$ double bond was deduced from the

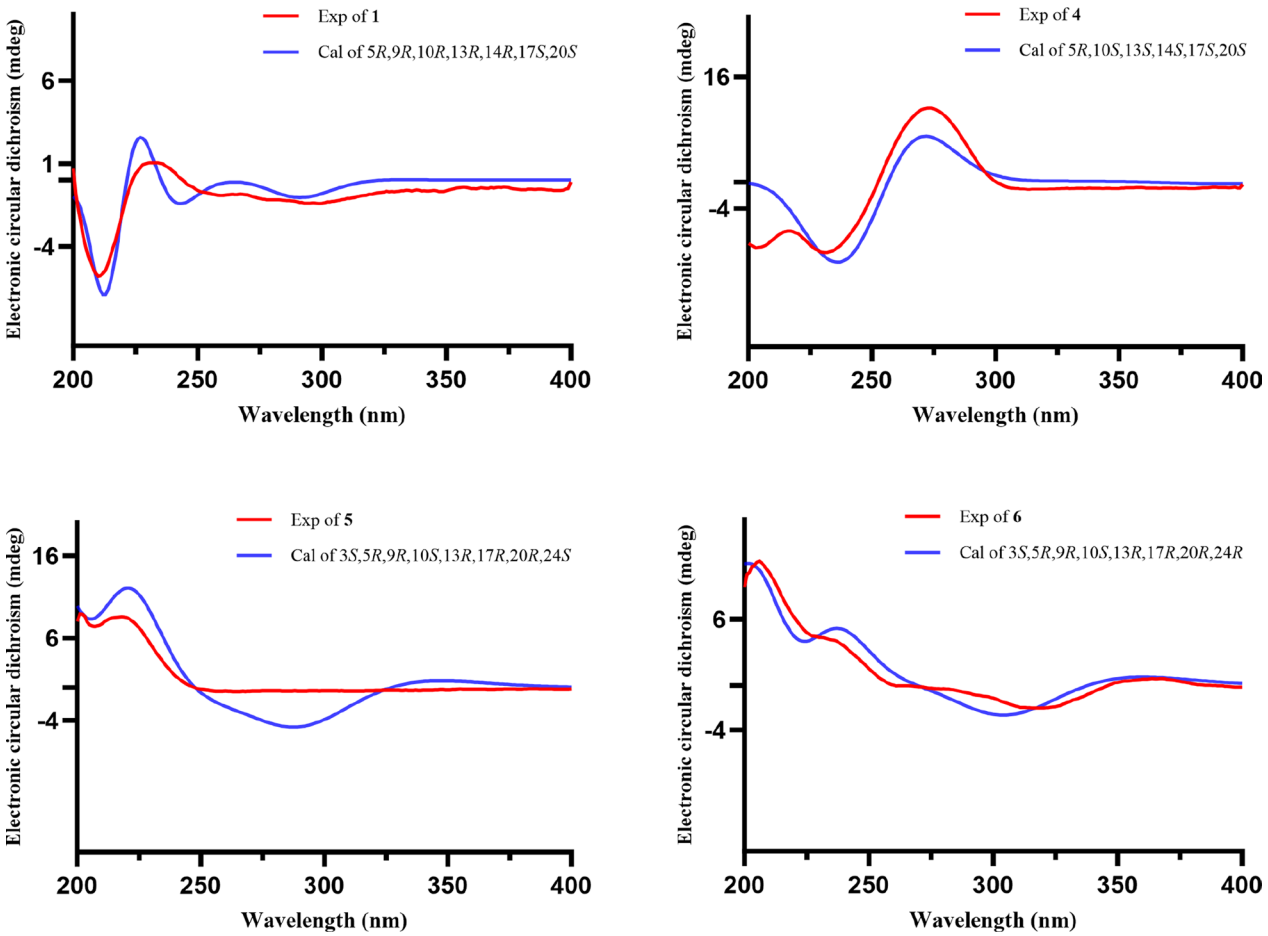

Fig. 4 Experimental and calculated ECD curves of compounds **1** and **4**–**6**

large coupling constant between the olefinic protons (δ_H 5.14, 1H, dd, J=16.0, 8.2 Hz; δ_H 5.14, 1H, dd, J=16.0, 8.2 Hz). The observed NOESY correlations between H-3/H-5, H-5/H-9, and H-9/H-17, determined that H-5, H-9, and H-17 were all located on the α-face of the steroid. Furthermore, the correlations between H_3-18/H_3-19 and H_3-18/H-20 confirmed the β-orientation of C-18, C-19, and C-20 (Fig. 3). Based on the above evidence, the structure of **5** was unambiguously determined to be (3*S*,8*E*,22*E*)-hydroxystigmast-8,22-diene-7,15-dione.

Coggygrerol B (**6**) was a yellowish gum, and its HRESIMS showed *m/z* 465.3334 $[M+Na]^+$, indicating a molecular formula of $C_{29}H_{46}O_3$. By comparing the spectroscopic data (Table 2) of **6** with those of **5**, it was found that **6** had a structure similar to that of **5**, except that the double bond $\Delta^{22,23}$ was absent in **6**. The main difference in the ^{1}H NMR spectrum was the absence of double bonds at δ_H 5.14 (2H), which was supported by the ^{13}C NMR spectrum. These changes were verified via the ^{1}H-^{1}H COSY correlations (Fig. 2) of H-20/H_2-22/H_2-23/H-24, together with the HMBC relationships (Fig. 2) of H-20, H_3-21 with C-22, and H-24, H_2-25 with C-23. Thus, the structure of **6** was determined as (3*S*,8*E*)-hydroxystigmast-8-ene-7,15-dione.

By comparing spectroscopic data with those reported previously, the 27 known compounds isolated from this plant were shown to be aglaiabbreviatin E (**7**) [19], 3,7-dioxo-8,24*Z*-tirucalladien-26-oic acid (**8**) [21], 3-hydroxy-7-oxo-8,24*Z*-tirucalladien-26-oic acid (**9**) [21], 7,11-dioxo-3-hydroxy-8,24*Z*-tirucalladien-26-oic acid (**10**) [21], isomasticadienoic acid (**11**) [22], 24*Z*-isomasticadienolic acid (**12**) [23], (9*R*)-3,6-dioxo-tirucalla-7,24*Z*-dien-26-oic acid (**13**) [24], 3-hydroxy-6-oxo-7,24*Z*-tirucalladien-26-oic acid (**14**) [21], masticadienonic acid (**15**) [23], schinol (**16**) [21], 28-norolean-16,18-dien-3-one (**17**) [25], oleana-11:l3(18)-dien-3β-ol, (**18**) [26], β-amyrin (**19**) [27], cycloeucalenol (**20**) [28], obtusifolione (**21**) [29], obtusifoliol (**22**) [30], citrostadienol (**23**) [31], β-sitosterol (**24**) [32], 6-hydroxystigmast-4-en-3-one (**25**) [33], ergosta-4,6,8(14),22-tetraen-3-one (**26**) [34], butein (**27**) [35], sulfuretin (**28**) [36], 3,3',5',5,7-pentahydroflavanone (**29**) [37],

Table 2 ^{1}H NMR(400 MHz) and ^{13}C NMR (100 MHz) data of **5** and **6** in $CDCl_3$

No	5		6	
	δ_H	δ_C	δ_H	δ_C
1	1.79 (m)	36.1	1.78 (m)	36.1
	1.21 (m)		1.21 (m)	
2	1.90 (d, 13.0)	30.9	1.88 (m)	30.9
	1.44 (m)		1.42 (m)	
3	3.65 (m)	70.5	3.64 (m)	70.5
4	1.72 (m)	37.8	1.72 (m)	37.8
	1.42 (m)		1.42 (m)	
5	1.67 (m)	44.3	1.67 (m)	44.3
6	2.53 (d, 13.7)	46.5	2.53 (d, 14.1)	46.5
	2.35 (dd, 13.7, 3.3)		2.36 (dd, 14.1, 3.5)	
7		202.1		202.3
8		143.0		143.2
9	2.12 (m)	51.3	2.10 (m)	51.2
10		38.4		38.4
11	1.74 (m)	19.7	1.72 (m)	19.6
	1.57 (m)		1.56 (m)	
12	2.09 (m)	35.8	2.10 (m)	35.8
	1.34 (m)		1.29 (m)	
13		42.1		42.3
14		148.4		148.4
15		205.1		205.4
16	2.44 (dd, 19.6, 8.4)	41.6	2.53 (dd, 19.3, 8.4)	40.9
	2.00 (dd, 19.6, 11.8)		2.01 (dd, 19.3, 11.6)	
17	1.73 (m)	51.0	1.70 (m)	51.0
18	1.01 (s)	18.2	1.00 (s)	18.1
19	0.95 (s)	12.5	0.95 (s)	12.5
20	2.23 (dd, 16.3, 7.2)	40.0	1.57 (m)	35.3
21	1.10 (d, 7.2)	21.7	1.01 (d, 7.8)	19.2
22	5.14 (dd, 16.0, 8.2)	136.2	1.29 (m)	33.6
			1.12 (m)	
23	5.14 (dd, 16.0, 8.2)	131.6	1.15 (m)	25.7
24	1.55 (m)	51.4	0.91 (m)	45.8
25	1.42 (m)	25.3	1.46 (m)	29.1
	1.15 (m)			
26	0.79 (d, 6.9)	12.4	0.83 (d, 6.8)	12.1
27	1.54 (m)	31.9	1.22 (m)	23.2
28	0.83 (d, 6.4)	21.2	0.81 (d, 6.4)	19.0
29	0.79 (d, 6.4)	19.3	0.83 (d, 6.4)	19.9

fustin (**30**) [38], (−)-butin (**31**) [36], (+)-butin (**32**) [35], And 5-hydroxyflavanone (**33**) [39].

2.2 Effect of compounds on the LPS induced production of NO

Various diseases are accompanied by inflammation, and identifying small-molecule natural products with anti-inflammatory activity is a promising strategy for developing novel and effective therapeutic agents. Thus, the inhibitory effects of compounds **1**−**27** on LPS induced NO production in RAW 264.7 cells were assessed. Among them, compounds **5**, **13**, **15**, **21**, and **26** exhibited inhibitory activities in LPS induced RAW 264.7 cells, with IC_{50} values ranging from 6.81 ± 0.15 to 21.54 ± 0.35 μM (Table 3). Notably, compound **15** exhibited activity comparable to that of the positive control dexamethasone (IC_{50}:8.25 ± 0.6 μM). Molecular docking analysis revealed that compound **15** has a high affinity for NLRP3 and iNOS, with binding energies of −11.7 and −10.3 kcal/mol, respectively (Fig. 5). The above findings confirms that **15** exerts its anti-inflammatory effect by acting on NLRP3 and iNOS, revealing that NLRP3 and iNOS may be potential targets for the inhibitory activities of compound **15** in LPS-induced RAW 264.7 cells. These findings suggested that Coggygrerol A (**5**), (9*R*)-3,6-dioxo-tirucalla-7,24*Z*-dien-26-oic acid (**13**), masticadienonic acid (**15**), obtusifolione (**21**) and ergosta-4,6,8(14),22-tetraen-3-one (**26**) exhibited notable anti-inflammatory effects.

Table 3 Inhibitory effects of compounds on NO production induced by LPS in RAW 264.7 cells

Compound	IC_{50} (μM)[a]
5	15.38 ± 0.20
13	11.26 ± 0.24
15	6.81 ± 0.15
21	21.54 ± 0.35
26	16.75 ± 0.44
Dexamethasone[b]	8.25 ± 0.6

[a] Half-inhibitory concentrations (IC_{50}) in μM

[b] Positive control

2.3 Antibacterial activity of the isolated compounds in vitro

The inhibitory effects of the 27 triterpenoid And sterol compounds against the 10 bacterial strains were evaluated, and the results are presented in Table 4. Compounds **3**, **4**, **10**, **13**, **14**, and **26** exhibited varying inhibitory effects against the tested bacteria, while the other compounds showed no significant inhibitory effects. Notably, all six compounds contain multiple carbonyl groups and conjugated systems, which are thought to be related to their antibacterial activities. Specifically, compound **3** demonstrated noteworthy antibacterial activity against MRSA ATCC BAA-1717(USA300) And MRSA 12228, exhibiting a MIC value of 8 μg/mL.

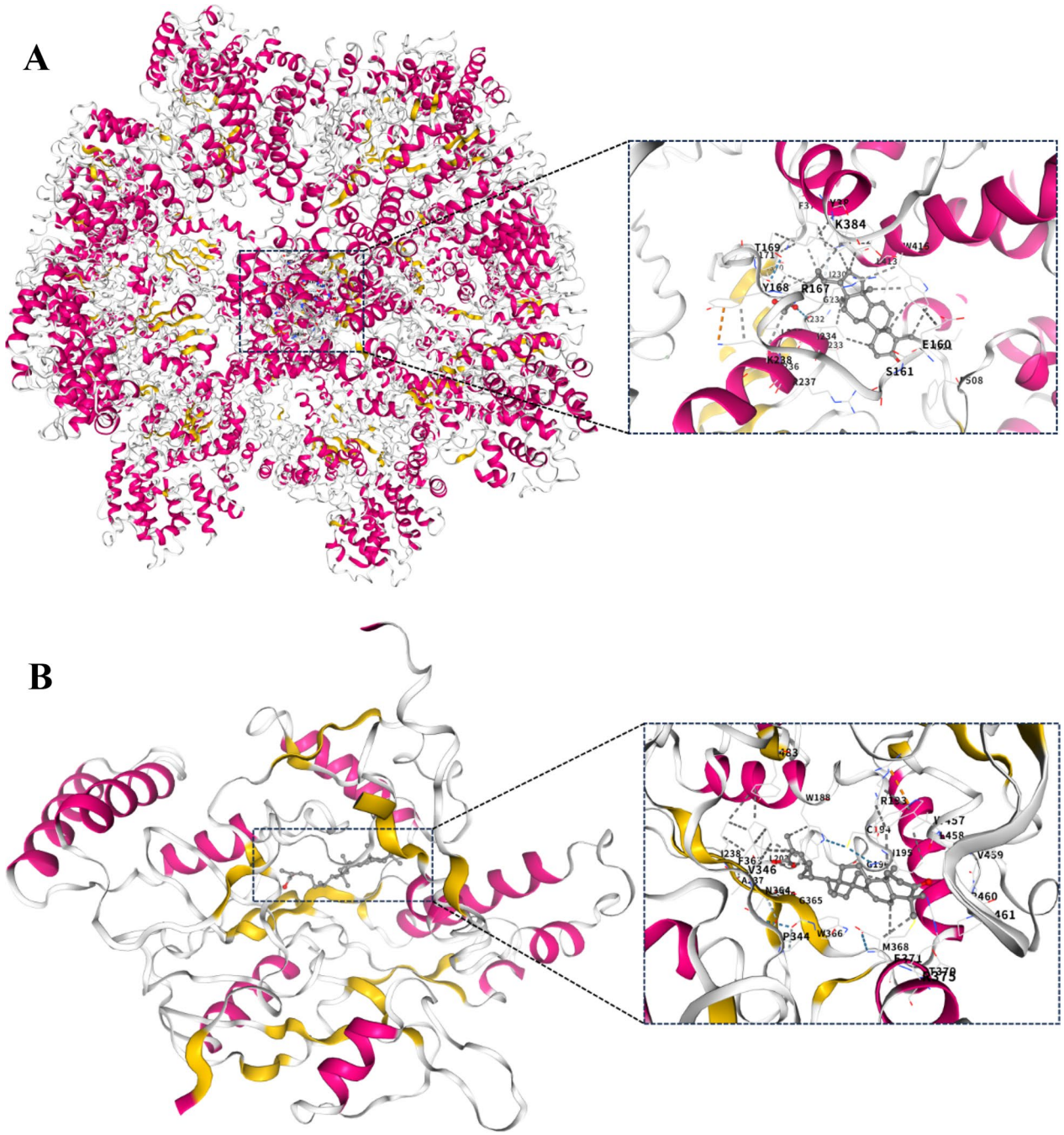

Fig. 5 The molecular interactions of compound **15** with NLRP3 (A) and iNOS (B) by molecular docking simulation

2.4 Inhibitory effect of compound 3 on the growth of MRSA ATCC BAA-1717(USA300)

The growth curves for MRSA ATCC BAA-1717(USA300) treated with compound **3** are shown in Fig. 6A. In the negative control group, the OD_{600} first increased rapidly And then remained stable until the end of the experiment. Compared to the control, 0.25 × MIC And 0.5 × MIC of **3** against MRSA ATCC

Table 4 Antibacterial activity of compounds against test bacteria

No	MIC (μg/mL)									
	G + bacteria					G- bacteria				
	S.a.[a]	*S.a.*[b]	*S.a.*[c]	*S.a.*[d]	*S.a.*[e]	*E.c.*[f]	*E.c.*[g]	*P.a.*[h]	*P.a.*[i]	*A.b.*[j]
3	16	8	8	16	32	128	64	64	> 128	64
4	16	16	32	16	64	> 128	128	64	128	64
10	128	64	64	128	128	> 128	> 128	> 128	64	> 128
13	32	32	128	64	64	64	128	128	> 128	64
14	64	64	> 128	> 128	128	> 128	> 128	128	64	> 128
26	64	16	16	32	64	32	32	64	128	32
ampicillin[k]	4	2	16	8	4	1	16	8	4	2
vancomycin[k]	1	0.5	1	0.5	1	8	4	4	2	8

[a] Methicillin-resistant *S. aureus* 171

[b] Methicillin-resistant *S. aureus* ATCC BAA-1717(USA300)

[c] Methicillin-resistant *S. aureus* ATCC 12228

[d] Methicillin-resistant *S. aureus* 209

[e] *S. aureus* ATCC 29213

[f] *E. coli* CMCC 44103

[g] *E. coli* CMCC 25922

[h] Multi-drug-resistant *P. aeruginosa* 110

[i] Multi-drug-resistant *P. aeruginosa* 174

[j] *A. baumannii* ATCC 19606

[k] Positive control

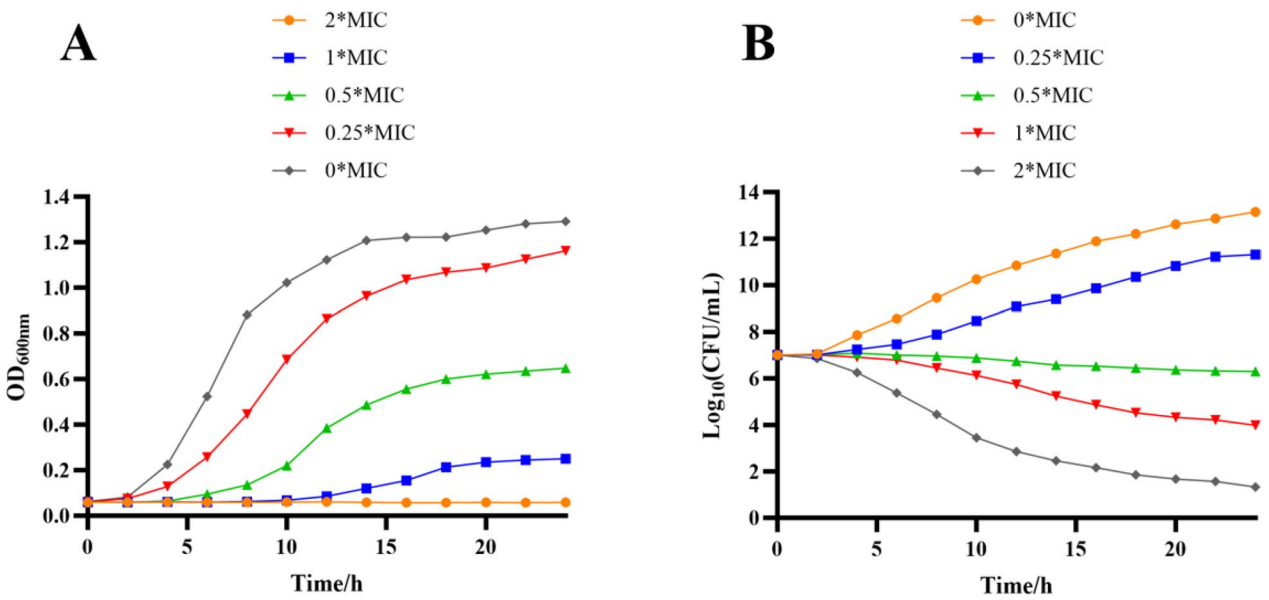

Fig. 6 Growth curves (**A**) and Time-kill curves (**B**) of compound **3** against MRSA ATCC BAA-1717 (USA300)

BAA-1717(USA300) slightly delayed the exponential phase of the bacterial cells. The logarithmic period of the cells was significantly delayed when a higher concentration of compound **3** (1 × MIC) was used. In addition, at 2 × MIC of **3** against MRSA171, the growth curve remained almost horizontal from beginning to end (i.e., no logarithmic period occurred), suggesting that the growth of the cells was completely inhibited (Fig. 6A). Consequently, the growth curve analysis revealed that compound **3** exhibited potent dose- and

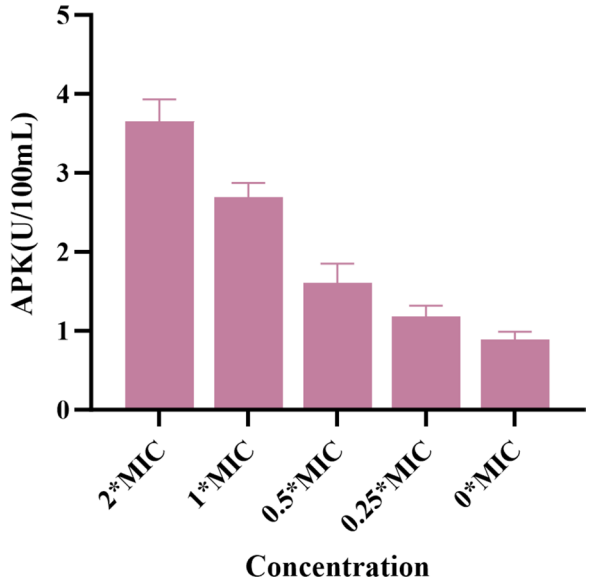

Fig. 7 The effect of compound **3** on AKP activity in MRSA ATCC BAA-1717 (USA300)

time-dependent inhibitory effects against MRSA ATCC BAA-1717(USA300).

2.5 Killing kinetics evaluation of compound 3 against MRSA ATCC BAA-1717(USA300)

In addition to the inhibition of bacterial growth, the rapid killing of bacteria is also a significant indicator of the antimicrobial activity of compounds. Consequently, compound **3** was selected for further evaluation of its bactericidal performance using a standard time-kill assay against MRSA ATCC BAA-1717(USA300). As illustrated in Fig. 6B, compound **3** rapidly eliminated MRSA ATCC BAA-1717(USA300) at 1×MIC And 2×MIC.

2.6 Extracellular alkaline phosphatase (AKP) activity

The assessment of extracellular AKP levels can serve as a rapid indicator of cell wall damage and functional disruption. In this study, extracellular AKP levels were measured to evaluate the extent of cell wall damage caused by **3**. As shown in Fig. 7, the AKP level increased with the concentration of **3**. Compared to the blank control group, the AKP levels in the bacterial samples increased significantly. These findings suggest that **3** disrupts the cell wall, leading to AKP release.

2.7 Antibiofilm activity

The effect of **3** on the biofilm formation capacity of MRSA ATCC BAA-1717(USA300) was evaluated using a crystal violet staining assay. Compound **3** exhibited a significant inhibitory effect on the biofilm formation of MRSA ATCC BAA-1717 (USA300). When treated with

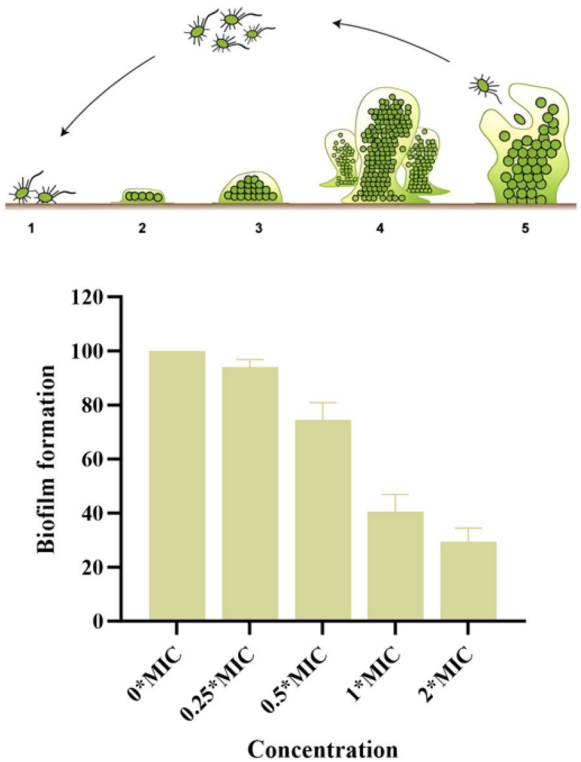

Fig. 8 The effect of compound **3** on biofilm formation in MRSA ATCC BAA-1717 (USA300)

3 at 2×MIC, biofilm formation was inhibited by 70.5%. Treatment with **3** at 1×and 1/2×MIC inhibited biofilm formation by 59.4% And 25.5%, respectively (Fig. 8).

2.8 SEM analysis of MRSA ATCC BAA-1717(USA300)

To further demonstrate the effects of **3** against MRSA ATCC BAA-1717(USA300), morphological alterations in the bacteria after treatment with **3** were examined using a Scanning Electron Microscope (SEM), and the resulting images are depicted in Fig. 9. Untreated MRSA ATCC BAA-1717(USA300) cells exhibited intact and smooth cell surfaces (Fig. 9A), whereas MRSA ATCC BAA-1717(USA300) cells treated with compound **3** at 4×the MIC exhibited severe damage and breakage (Fig. 9B). According to these SEM results, it was inferred that the possible antibacterial mechanism of **3** against MRSA ATCC BAA-1717(USA300) might involve the induction of abnormal morphology in the cell membranes, causing an increase in membrane permeability.

2.9 Combination susceptibility testing

Combination susceptibility testing revealed that **3** and ampicillin exerted an additive effect against MRSA ATCC BAA-1717(USA300) (Fig. 10). This combination targets

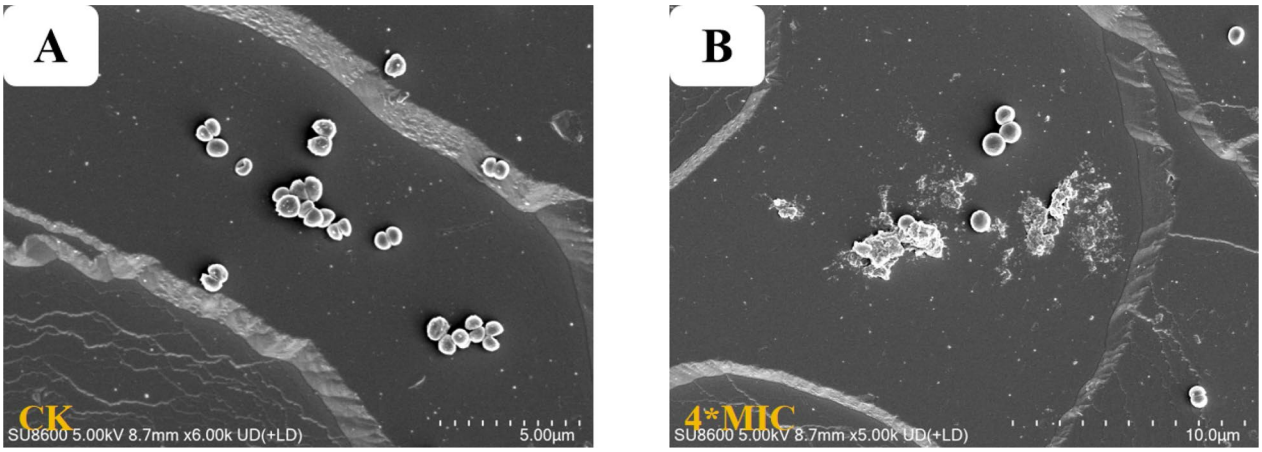

Fig. 9 Scanning electron microscopy (SEM) images of MRSA ATCC BAA-1717 (USA300) treated with compound **3**. **A** Control for MRSA ATCC BAA-1717 (USA300). **B** Treated by compounds **3**

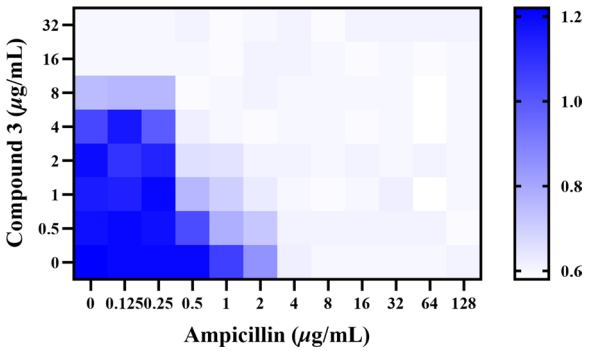

Fig. 10 Antibacterial effect of the combination of compound **3** and ampicillin against MRSA ATCC BAA-1717 (USA300)

multiple bacterial sites, thereby reducing the likelihood of simultaneous resistance development to both mechanisms. Moreover, the use of this combination may enable dose reduction of each individual agent, potentially minimizing toxicity and delaying the emergence of resistance.

2.10 Antibacterial activity of compound 3 in *vivo* in the *G. mellonella* infection model

Based on the excellent antibacterial activity of compound **3**, it was further evaluated in *vivo* using a *G. mellonella* infection model with vancomycin as the positive control, as in the in *vitro* experiments. As shown in Fig. 11, treatment with **3** significantly increased the survival rate and reduced the bacterial content in the body in a dose-dependent Manner from 5 to 20 mg/kg. Moreover, at the high dose of 20 mg/kg, the treatment rate was 80%, consistent with that of the positive control group. These findings suggest that compound **3** has potential as a candidate for future antibiotic development.

3 Conclusion

Six previously unreported compounds, triterpenoids (**1**–**4**) and sterols (**5** and **6**) And 27 known compounds (**7**–**33**) were isolated and identified from *C. coggygria*. Anti-inflammatory bioactivity evaluation showed that compounds **5**, **13**, **15**, **21**, and **26** significantly inhibited NO production induced by LPS in RAW264.7 cells, with IC_{50} values ranging from 6.81 ± 0.15 And 21.54 ± 0.35 μM. The molecular docking results indicated the potential of NLRP3 and iNOS as target proteins for compound **15**. Furthermore, the isolated triterpenoids and sterols were evaluated for their antibacterial activity against ten bacterial strains, revealing that compound **3** was the most active, with significant inhibitory activity against MRSA ATCC BAA-1717 (USA300). Subsequent analysis of the antibacterial mechanism indicated that compound **3** could potentially lead to the destruction of bacterial cell walls and membranes. Additionally, a synergistic effect was observed when **3** was combined with ampicillin. Compound **3** also exhibited antibacterial activity in a *G. mellonella* infection model. These findings provide a preliminary molecular and biological basis for the anti-inflammatory and antibacterial activities of small-molecule components in *C. coggygria*. In addition to being an ornamental tree species, *C. coggygria* may be developed as a value-added medicinal plant because of its highlighted antibacterial potential.

4 Experimental

4.1 General experimental procedures

The general experimental procedures were carried out in accordance with a previous report and are detailed in Text S1 [40].

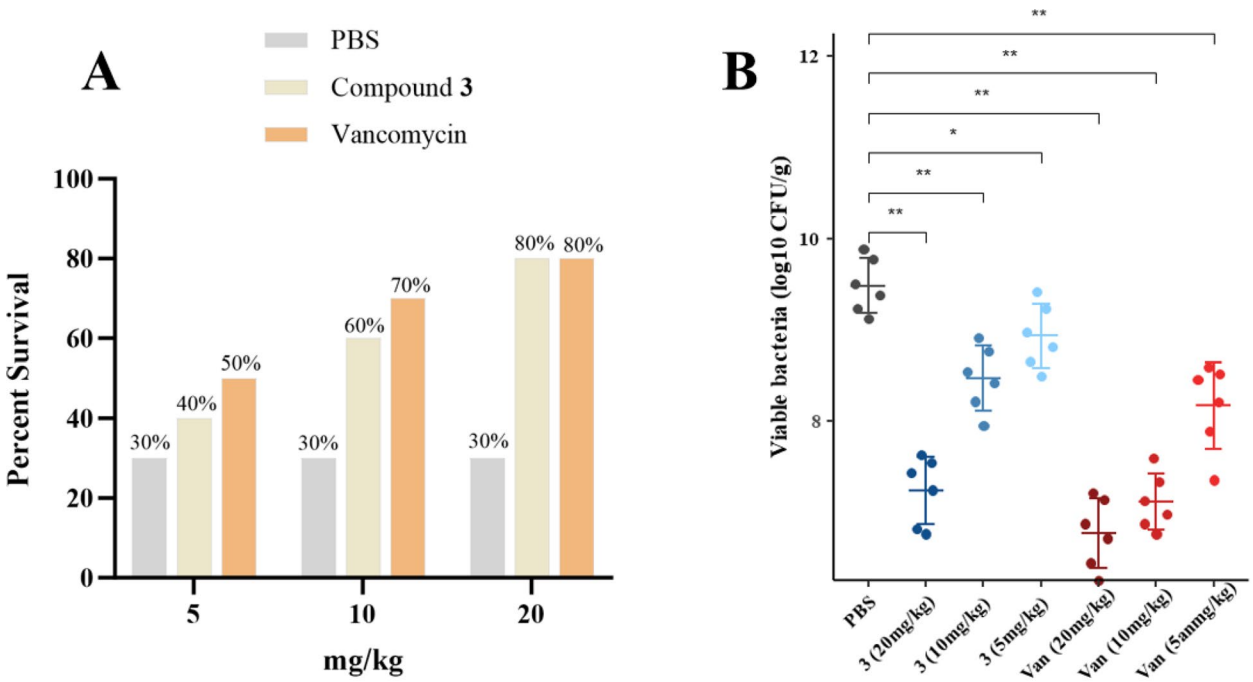

Fig. 11 In *vivo* antibacterial activity of compound **3**. **A** Survival rate of infected *G. mellonella* after treatment with different concentrations of the drug (n = 10). **B** Bacterial content in *G. mellonella* (n = 6)

4.2 Plant material

The tree stems and bark of *C. coggygria* were collected in October 2023 from the Tsinling Mountains of China. The plant species were identified by Dr. Zhen-Hai Wu, College of Life Sciences, Northwest A&F University. A voucher specimen (no. WUK 0480712) was deposited in the Herbarium of the College of Life Sciences, Northwest A&F University.

4.3 Extraction and isolation

The dried and crushed tree stems and bark of *C. coggygria* (30.0 kg) were subjected to three rounds of extraction with eight times their volume of heated 95% ethanol, resulting in a 4.5 kg crude extract. Subsequently, the crude extract was dissolved in three times the volume of water and partitioned sequentially with equal volumes of petroleum ether, and EtOAc, resulting in three partitions. Silica gel flash column chromatography (FCC) with dichloromethane/MeOH (80:1 to 2:1) was used to purify EtOAc fraction C (600.0 g), resulting in four fractions (A–D). Fraction A (30.0 g) was further purified using an FCC silica gel column and eluted with PE/EtOAc (40:1 to 0:1), resulting in five subfractions (A1–A5). Hereafter, A2 (1.4 g) was divided into four subfractions (A2-1–A2-4) using FCC silica gel with petroleum ether/EtOAc (20:1 to 2:1). The A2-1 (203.0 mg) and A2-2 (120.0 mg) fractions were separated by semipreparative HPLC to obtain compounds **3** (MeOH/H_2O, 95:5; flow rate: 2 mL/min; 3.5 mg; t_R = 22.2 min), **7** (MeOH/H_2O, 95:5; flow rate: 2 mL/min; 8.8 mg; t_R = 29.1 min), **16** (MeOH/H_2O, 98:2; flow rate: 2 mL/min; 7.6 mg; t_R = 18.2 min), and **17** (MeOH/H_2O, 98:2; flow rate: 2 mL/min; 18.0 mg; t_R = 25.0 min), respectively. Futher, Fraction A2-3 (60.0 g) was separated on a silica gel column eluted with PE/EtOAc (5:1) to give compounds **11** (10.5 mg) and **12** (7.6 mg). Fraction A3 (5.3 g) was separated on a silica gel column using PE/EtOAc (20:1 to 2:1) elution to yield subfractions A3-1 and A3-2. Fractions A3-1 (1.2 g) and A3-2 (1.9 g) were separated by chromatography on a Sephadex LH-20 column and eluted with dichloromethane/MeOH (1:1) and then purified using semi-preparative HPLC, which yielded compounds **4** (MeOH/H_2O, 90:10; flow rate: 2 mL/min; 10.8 mg; t_R = 20.1 min), **18** (MeOH/H_2O, 90:10; flow rate: 2 mL/min; 12.0 mg; t_R = 23.8 min), **19** (MeOH/H_2O, 92:8; flow rate: 2 mL/min; 35.0 mg; t_R = 23.1 min), **24** (MeOH/H_2O, 92:8; flow rate: 2 mL/min; 26.0 mg; t_R = 28.9 min), and **25** (MeOH/H_2O, 92:8; flow rate: 2 mL/min; 8.0 mg; t_R = 32.0 min). Fraction A4 (3.1 g) was separated on a silica gel column eluted with PE/EtOAc (20:1 to 1:1) to give fractions A4-1–A4-5. A4-1 (188.0 mg) was further separated on silica gel CC (PE/EtOAc, 12:1) followed by elution to yield **8** (18.4 mg), **9**

(22.0 mg), and **15** (10.8 mg). Fraction A4-2 (550.0 mg), on the other hand, was subjected to chromatography on Sephadex LH-20 (Me_2CO) and then purified using HPLC ($MeOH/H_2O$, 89:11), which yielded compound **1** (3.3 mg, $t_R = 45.8$ min) and **2** (2.8 mg, $t_R = 47.2$ min). A4-3 (1.1 g) was applied to silica gel CC eluted with a gradient of PE/EtOAc (20:1 to 5:1), to give five subfractions (A4-3–1−A4-3–4). Section A4-3–2 (65.0 mg) was purified by semipreparative HPLC ($MeOH/H_2O$, 85:15; flow rate: 2 mL/min) to yield compounds **5** (6.0 mg; $t_R = 26.6$ min) and **6** (6.5 mg; $t_R = 28.0$ min). Similarly, compounds **10** (4.5 mg; $t_R = 32.0$ min) and **13** (9.8 mg; $t_R = 35.2$ min) were isolated from subfraction A4-3–3 (320.0 mg) using semi-preparative HPLC ($MeOH/H_2O$, 86:14; flow rate: 2 mL/min). As well, A4-3–4 (980.0 mg) was subjected to Sephadex LH-20 column elution with MeOH to obtain subfractions A4-3-4-1 and A4-3-4-2. Compound **14** (26.0 mg; $t_R = 24.3$ min) was isolated from subfraction A4-3-4-1 (310.0 mg) by semipreparative HPLC ($MeOH/H_2O$, 81:19; flow rate: 2 mL/min). Additionally, compounds **20** (4.5 mg; $t_R = 20.8$ min), **21** (5.0 mg; $t_R = 34.5$ min), and **26** (85.0 mg; $t_R = 38.0$ min) were isolated from A4-3-4-2 (525.0 mg) by semipreparative HPLC ($MeOH/H_2O$, 84:16; flow rate: 2 mL/min). Fraction B (15.0 g) was isolated using silica gel CC (PE/EtOAc, 20:1 to 1:1) to obtain three fractions (B1−B3). B1 (1.5 g) was then purified over a Sephadex LH-20 column and eluted with dichloromethane/MeOH to afford B1-1− B1-4. Separation of B1-2 (160.0 mg) on semipreparative HPLC ($MeOH/H_2O$, 88:12; flow rate: 2 mL/min) afforded compounds **22** (12.8 mg; $t_R = 20.6$ min) and **23** (3.8 mg; $t_R = 23.9$ min). Fraction C (300.0 g) was separated on a silica gel column chromatograph using gradient elution (dichloromethane/MeOH, 40:1 to 5:1), yielding five subfractions (C1−C5). Fraction C2 (16.0 g) was further separated on a silica gel column and eluted with dichloromethane/MeOH (40:1 to 10:1) to obtain fractions C2-1−C2-6. Purification of fraction C2-2 (1.3 g) via semipreparative HPLC ($MeOH/H_2O$, 74:26; flow rate: 2 mL/min) yielded compounds **27** (7.5 mg; $t_R = 19.2$ min), **28** (4.6 mg; $t_R = 25.0$ min), **31** (75.0 mg; $t_R = 27.6$ min), **32** (86.0 mg; $t_R = 29.4$ min), and **33** (24.5 mg; $t_R = 35.2$ min). Fraction C2-3 (2.1 g) was purified by semi-preparative HPLC ($MeOH/H_2O$, 76:24; flow rate: 2 mL/min) to yield compound **29** (19.0 mg, $t_R = 20.0$ min)and **30** (46.0 mg; $t_R = 26.9$ min).

Coggygrnoid A (**1**): Colorless solid; $[\alpha]_{20}^{D}$+45.0 (*c* 0.1, MeOH); UV (MeOH) λmax (log *ε*): 228.0 (2.55) nm; CD (MeOH) λ_{max} (*Δε*) 210 (– 5.79), 233 (+1.05); ^{1}H and ^{13}C NMR data see Table 1; HRESIMS $[M+Na]^+$ *m/z* 461.3382 (calcd for $C_{30}H_{46}O_2Na$, 461.3390).

Coggygrnoid B (**2**): Colorless solid; $[\alpha]_{20}^{D}$+60.0 (*c* 0.1, MeOH); UV (MeOH) λ_{max} (log *ε*): 226.0 (2.29) nm; ^{1}H and ^{13}C NMR data see Table 1; HRESIMS $[M+Na]^+$ *m/z* 461.3395 (calcd for $C_{30}H_{46}O_2Na$, 461.3390).

Coggygrnoid C (**3**): Faint yellowish gum; $[\alpha]_{20}^{D}$+14.0 (*c* 0.1, MeOH); UV (MeOH) λ_{max} (log *ε*): 281.0 (2.30) nm; ^{1}H and ^{13}C NMR data see Table 1; HRESIMS $[M+Na]^+$ *m/z* 477.3330 (calcd for $C_{30}H_{46}O_3Na$, 477.3339).

Coggygrnoid D (**4**): Yellowish gum; $[\alpha]_{20}^{D}$−28.0 (*c* 0.1, MeOH); UV (MeOH) λ_{max} (log *ε*): 269.0 (2.13) nm; CD (MeOH) λ_{max} (*Δε*) 203 (– 9.99), 231 (– 10.71), 273 (+11.25); ^{1}H and ^{13}C NMR data see Table 1; HRESIMS $[M-H]^-$ *m/z* 481.2957 (calcd for $C_{30}H_{41}O_5$, 481.2959).

Coggygrerol A (**5**): Yellowish gum; $[\alpha]_{20}^{D}$+26.0 (*c* 0.1, MeOH); UV (MeOH) λ_{max} (log *ε*): 200.0 (2.52) nm; CD (MeOH) λ_{max} (*Δε*) 201 (+8.91), 218 (+8.58); ^{1}H and ^{13}C NMR data see Table 2; HRESIMS $[M+Na]^+$ *m/z* 463.3179 (calcd for $C_{29}H_{44}O_3Na$, 463.3183).

Coggygrerol B (**6**): Yellowish gum; $[\alpha]_{20}^{D}$+24.0 (*c* 0.1, MeOH); UV (MeOH) λ_{max} (log *ε*): 200.0 (2.34), 258.0 (1.98) nm; CD (MeOH) λ_{max} (*Δε*) 206 (+11.23), 319 (– 2.03), 273 (+11.25); ^{1}H and ^{13}C NMR data see Table 2; HRESIMS $[M+Na]^+$ *m/z* 465.3334 (calcd for $C_{29}H_{46}O_3Na$, 465.3339).

4.4 Anti-inflammatory assay

As outlined in our previous article, the MTT assay and Griess reaction were employed to measure cell viability and NO production [41]. Futhermore, Molecular docking studies was operated as described previously [41].

4.5 Anti-bacterial assay

The effects of compounds **1**−**27** against the five gram-positive bacteria (Methicillin-resistant *S. aureus* 171, Methicillin-resistant *S. aureus* ATCC BAA-1717 (USA300), Methicillin-resistant *S. aureus* ATCC 12228, Methicillin-resistant *S. aureus* 209, and *S. aureus* ATCC 29213) and five gram-negative bacteria (*E. coli* CMCC 44103, *E. coli* CMCC 25922, Multi-drug-resistant *P. aeruginosa* 110, Multi-drug-resistant *P. aeruginosa* 174, and *A. baumannii* ATCC 19606) were evaluated in *vitro*. The minimal inhibitory concentration (MIC) was determined for compounds **1**−**27** using the antibacterial activity test protocols described in previous reports [42]. Based on previously reported methods [42], the growth curve of MRSA171 treated with compound **3** were evaluated. The previously described method was used to determine the time-kill curve of the test bacteria [43].

4.6 Determination of alkaline phosphatase (AKP) activity

Following an 8-h co-incubation of MRSA ATCC BAA-1717 (USA300) with **3**, culture supernatants from each

treatment group were collected. The concentration of alkaline phosphatase (AKP) was subsequently determined using a commercial AKP assay kit, following the manufacturer's protocol [44].

4.7 Assay for biofilm suppression

MRSA ATCC BAA-1717 (USA300) was incubated with **3** for 24 h. After incubation, the medium was removed And the biofilms were washed twice with PBS. Then, 0.1% crystal violet solution was added to each well And incubated for 30 min. The dye was dissolved by adding 33% glacial acetic acid after staining. After incubating for 1 h, the absorbance at OD_{590} was determined using a microplate reader [45].

4.8 Scanning electron microscopy (SEM)

According to our method, with minor modifications [42], a scanning electron microscopy (SEM) study was conducted to observe the cellular morphological changes in MRSA ATCC BAA-1717 (USA300) treated with **3**. MRSA ATCC BAA-1717 (USA300) (approximately 2×10^8 CFU/mL) was treated with compound **3** at 4×MIC. After culturing for 10 h at 37 °C, MRSA ATCC BAA-1717 (USA300) was collected, washed with PBS (0.1 M, pH7.0) and then anchored with glutaraldehyde. Field-emission scanning electron microscopy (FE-SEM; Nova Nano SEM-450, FEI Instruments, Inc. Hillsboro, Oregon) was used for the microstructural evaluation of MRSA ATCC BAA-1717 (USA300).

4.9 Checkerboard MIC assay

The microdilution checkerboard method was used to evaluate the antibacterial effect of compound **3** in combination with ampicillin against MRSA ATCC BAA-1717 (USA300). Specifically, two-fold serial dilutions of **3** And ampicillin were prepared in a 96-well microtiter plate And inoculated with a bacterial suspension at a final concentration of 1×10^8 CFU/mL. After incubation at 37 °C for 24 h, the interaction between the two agents was assessed using the fractional inhibitory concentration index (FICI) formula [46].

$$\begin{aligned}\mathrm{FICI} &= (\mathrm{MIC_{A\ in\ combination}}/\mathrm{MIC_{A\ alone}}) \\ &+ (\mathrm{MIC_{B\ in\ combination}}/\mathrm{MIC_{B\ alone}})\end{aligned}$$

4.10 *G. mellonella* infection model and in vivo antibiotic activity assessment

G. mellonella larvae are used widely as surrogate infectious diseasemodels,due to ease ofuse and the presence of an innate immune system functionally similar to that of vertebrates [47]. To Analyze the survival of infected larvae, 5 μL of the bacterial inoculum (1×10^8 CFU/mL) was injected dorsolaterally into the hemocoel of the last-instar larvae. Following An incubation period at 37 °C for 60 min And observation that the larvae continued to survive normally, 5 μL of each working solution of compound **3** or the positive drugs (5, 10, And 20 mg/kg) were injected. The larvae were deemed deceased when they exhibited An absence of tactile response following a 72-h incubation at 37 °C. Similarly, the second batch of *G. mellonella* was inoculated with bacteria And treated with different concentrations of the drug using the same method as above. After 24 h, the entire *G. mellonella* homogenate was suspended in PBS, then serially diluted tenfold to 10^8-fold. A 100 μL aliquot was spread onto agar plates, And colony counts were performed after 18 h (expressed in $\log^{10}$ CFU/g).

4.11 Statistical analysis

All of the biological experimental data presented in this paper were replicated three times, and the results are shown as the mean ± standard deviation (SD).

Supplementary Information

The online version contains supplementary material available at https://doi.org/10.1007/s13659-025-00553-4.

Additional file 1.

Acknowledgements
This research was financially supported by the National Natural Science Foundation of China (No. 32201249, 22277099, 22077102, 32070388), the Qin ChuangYuan "Scientists+Engineers" Team Construction Project (No. 2023KXJ-214), the Shaanxi Province Innovation Support Project (2025ZY1-GNYZ-13), the Shaanxi Administration of Traditional Chinese Medicine (No. 2022-09-20), and the Northwest A&F University "Double First-Class" Construction Project. The Advance Analysis and Measurement Center of Northwest A&F University helped us measure the NMR and MS spectra.

Author contributions
YT-Z: performing separation, purification and structural identification and wrote this manuscript. ZR-L: testing NMR and HRESIMS data. JH-L: testing the anti-inflammatory activity. RH-C and W-W: testing the anti-bacterial activit. YQ-G, CH-L and JM-G: designed this research work and provided funding support. All authors have read and agreed to publish the manuscript.

Funding
This research was funded by the National Natural Science Foundation of China (No. 32201249, Chun-Huan Li, 22277099, Jin-Ming Gao, 22077102, Jin-Ming Gao, 32070388, Jin-Ming Gao)

Data availability
Upon reasonable request, data utilised or analysed during this study may be obtained from the corresponding author.

Declarations

Competing interests
All the authors declare no competing financial interest.

Author details
[1]Shaanxi Key Laboratory of Natural Products & Chemical Biology, College of Chemistry & Pharmacy, Northwest A&F University, Yangling 712100, People's Republic of China. [2]College of Food Science and Technology, Northwest University, Xi'an, Shaanxi 710069, People's Republic of China.

Received: 31 July 2025 Accepted: 6 September 2025
Published: 5 January 2026

References

1. Editorial Committee of the Flora of China, Chinese Academy of Sciences. Flora of China. 1980; 45: 96–99
2. Tzakou l, Bazos A. Essential oils of leaves, inflorescences and infructescences of spontaneous *Cotinus coggygria* Scop. from Greece. Flavour Fragr J. 2005;20(5):531–3.
3. Antal DS, Schwaiger S, Ellmerer-Müller EP, Stuppner H. *Cotinus coggygria* wood: novel flavanone dimer and development of an HPLC/UV/MS method for the simultaneous determination of fourteen phenolic constituents. Planta Med. 2010;76(15):1765–72.
4. Westenburg HE, Lee KJ, Lee SK, Fong HH, vanBreemen RB, Pezzuto JM, et al. Activity-guided isolation of antioxidative constituents of *Cotinus coggygria*. J Nat Prod. 2000;63(12):1696–8.
5. Demirci BETÜL, Demirci FATİH, Başer KHC. Composition of the essential oil of *Cotinus coggygria* Scop. from Turkey. Flavour Fragr J. 2003;18(1):43–4.
6. Nićiforović N, Mihailović V, Mašković P, Solujić S, Stojković A, Muratspahić DP. Antioxidant activity of selected plant species; potential new sources of natural antioxidants. Food Chem Toxicol. 2010;48(11):3125–30.
7. Ivanova D, Gerova D, Chervenkov T, Yankova T. Polyphenols and antioxidant capacity of Bulgarian medicinal plants. J Ethnopharmacol. 2005;96(1–2):145–50.
8. Long L, Ma Z, Cui E, Han C, Zhang L, Zhang B. Research on depressurization effect of *cotinus coggygria*. Chin J Lab Diagn. 2009;13:330–1.
9. Constantin RP, Constantin J, Pagadigorria CLS, Ishii-Iwamoto EL, Bracht A, Ono MDKC, et al. The actions of fisetin on glucose metabolism in the rat liver. Cell Biochem Funct. 2010;28(2):149–58.
10. Marčetić M, Božić D, Milenković M, Malešević N, Radulović S, Kovačević N. Antimicrobial, antioxidant and anti-inflammatory activity of young shoots of the smoke tree, *Cotinus coggygria* Scop. Phytother Res. 2013;27(11):1658–63.
11. Liu WY, Qiu H, Li HM, Zhang R, Pan YK, Cao CY, et al. Prenylated flavonoids from *Hypericum perforatum* L. and their anti-neuroinflammatory and neuroprotective activities. Ind Crops Prod. 2024;216:118792.
12. Liu WY, Gao LL, Zhou W, Ma YN, Tian JM, Gao JM. Hypertums a-j, bioactive polycyclic polyprenylated acylphloroglucinols with diverse skeletons from *Hypericum perforatum* L. (St. John's wort). Phytochemistry. 2025;235:114450.
13. Liu WY, Lei XX, Wang WJ, Tian JM, Gao YQ, Gao JM. Hyperforatone A, the 1, 8-seco rearranged polycyclic polyprenylated acylphloroglucinol with a unique bicyclo [5.4.0] undecane core from *Hypericum perforatum*. Chin Chem Lett. 2025;36(4):110478.
14. Tang JJ, Huang LF, Deng JL, Wang YM, Guo C, Peng XN, et al. Cognitive enhancement and neuroprotective effects of OABL, a sesquiterpene lactone in 5xFAD Alzheimer's disease mice model. Redox Biol. 2022;50:102229.
15. Xie JY, Li P, Yan XT, Gao JM. Discovery from *hypericum elatoides* and synthesis of hyperelanitriles as *α*-aminopropionitrile-containing polycyclic polyprenylated acylphloroglucinols. Commun Chem. 2024;7(1):1–1.
16. Xie JY, Gao YQ, Liu WY, Zhang SY, Li D, Wang WJ, Tang JJ, Gao JM. Hypertaxoids A and B, two unique meroterpenoids from Hypericum elatoides as microtubule stabilizers and their antiproliferative effects on cervical cancer. Chin Chem Lett. 2025;111580. https://doi.org/10.1016/j.cclet.2025.111580.
17. Xie JY, Wang ZX, Liu WY, Liu HW, Li D, Sang YF, et al. Hyperelatolides A-D, antineuroinflammatory constituents with unusual carbon skeletons from *Hypericum elatoides*. J Nat Prod. 2023;86(8):1910–8.
18. Quang DN, Long LD, Tung NQ, Thanh NN, Tham LX. Endertiins A-B, two lanostane triterpenoids from the fruit bodies of the mushoom *Humphreya endertii*. Nat Prod Res. 2022;36(6):748–53.
19. Zhang F, Wang JS, Gu YC, Kong LY. Triterpenoids from *Aglaia abbreviata* and their cytotoxic activities. J Nat Prod. 2010;73(12):2042–6.
20. Xu JL, Gu LH, Wang ZT, Bligh A, Han ZZ, Liu SJ. Seventeen steroids from the pith of *Tetrapanax papyriferus*. J Asian Nat Prod Res. 2016;18(12):1131–7.
21. Makino M, Motegi T, Fujimoto Y. Tirucallane-type triterpenes from *Juliania adstringens*. Phytochemistry. 2004;65(7):891–6.
22. Ono M, Yamashita M, Mori K, Masuoka C, Eto M, Kinjo J, et al. Sesquiterpenoids, triterpenoids, and flavonoids from the fruits of *Schinus molle*. Food Sci Technol Res. 2008;14(5):499–499.
23. Mulholland DA, Nair JJ. Triterpenoids from *Dysoxylum pettigrewianum*. Phytochemistry. 1994;37(5):1409–11.
24. Liu W, Gao J, Li M, Aisa HA, Yuan T. Tirucallane triterpenoids from the mastic (*Pistacia lentiscus*) and their anti-inflammatory and cytotoxic activities. Phytochemistry. 2021;182:112596.
25. An XR, Feng YP, Sun YW, Yang X, Liu W, Yuan T. A new nortriterpenoid from mastic. China J Chin Mater Med. 2024;49(23):6342–51.
26. Tanaka R, Matsunaga S. Triterpene dienols and other constituents from the bark of *Phyllanthus flexuosus*. Phytochemistry. 1988;27(7):2273–7.
27. Kajikawa M, Yamato KT, Fukuzawa H, Sakai Y, Uchida H, Ohyama K. Cloning and characterization of a cDNA encoding *β*-amyrin synthase from petroleum plant *Euphorbia tirucalli* L. Phytochemistry. 2005;66(15):1759–66.
28. Wen L, Weiming C, Zhi X, Xaotain L. New triterpenoids of *Pholidota chinensis*. Planta Med. 1986;52(1):4–6.
29. Ferreira MJ, Lobo AM, Nascimento JM, Wyler H. Tetra-and pentacyclic triterpenes from the aerial parts of *Euphorbia piscatoria*. Planta Med. 1994;60(6):581–2.
30. Shirane N, Murabayashi A, Masuko M, Uomori A, Yoshimura Y, Seo S, et al. Effect on ergosterol biosynthesis of a fungicide, SSF-109, in *Botrytis cinerea*. Phytochemistry. 1990;29(8):2513–20.
31. Kim JS, Yean MH, Lee SY, Lee JH, Kang SS. Phytochemical studies on *Lonicera caulis* (3)-iridoids. Korean J Pharmacogn. 2009;40(4):334–8.
32. Li YH, Luo F, Peng SL, Liang J, Ding LS. A new dihydroisocoumarin from the rhizomes of *Notopterygium forbesii*. Nat Prod Res. 2006;20(9):860–5.
33. Sun XB, Zhao PH, Xu YJ, Sun LM, Cao MA, Yuan CS. Chemical constituents from the roots of *Polygonum bistorta*. Chem Nat Compd. 2007;43(5):563–6.
34. Gan KH, Kuo SH, Lin CN. Steroidal constituents of *Ganoderma applanatum* and *Ganoderma neo-japonicum*. J Nat Prod. 1998;61(11):1421–2.
35. Prachayasittikul S, Buraparuangsang P, Worachartcheewan A, Isarankura-Na-Ayudhya C, Ruchirawat S, Prachayasittikul V. Antimicrobial and antioxidative activities of bioactive constituents from *Hydnophytum formicarum* Jack. Molecules. 2008;13(4):904–21.
36. Junior GMV, deMSousa CM, Cavalheiro AJ, Lago JHG, Chaves MH. Phenolic derivatives from fruits of *Dipteryx lacunifera* Ducke and evaluation of their antiradical activities. Helv Chim Acta. 2008;91(11):2159–67.
37. Zhou L, Li D, Wang J, Liu Y, Wu J. Antibacterial phenolic compounds from the spines of *Gleditsia sinensis* Lam. Nat Prod Res. 2007;21(4):283–91.
38. Shrestha S, Lee DY, Park JH, Cho JG, Lee DS, Li B, et al. Flavonoids from the fruits of Nepalese sumac (*Rhus parviflora*) attenuate glutamate-induced neurotoxicity in HT22 cells. Food Sci Biotechnol. 2013;22(4):895–902.
39. Haraguchi H, Tanaka Y, Kabbash A, Fujioka T, Ishizu T, Yagi A. Monoamine oxidase inhibitors from *Gentiana lutea*. Phytochemistry. 2004;65(15):2255–60.
40. Shi YF, Zhu YT, Zhang ZH, Chen MS, Gao S, Zhang Q, et al. Structurally diverse chromane meroterpenoids from *Rhododendron capitatum* with multifunctional neuroprotective effects. Eur J Med Chem. 2025;283:117188.
41. Yang JR, Zhu YT, Zeng YQ, Li HQ, Li CH, Gao JM. Three new ionone glycosides from *rhododendron capitatum* maxim. Molecules. 2024;29(11):2462.
42. Chen XM, Lu W, Zhang ZH, Wang PP, Zhang XJ, Xiao CJ, et al. Discovery of diversified cassane diterpenoids as potent antibacterial agents from *Caesaplinia pulcherrima* and their mechanisms. Pest Manag Sci. 2023;79(7):2539–55.
43. Guo W, Yang Z, Wang K, Li W, Zhao Y, Yang Y, et al. Discovery of unique bis-substituted aromatic amide derivatives as novel highly potent antibiotics for combating methicillin-resistant *Staphylococcus aureus* (MRSA). J Med Chem. 2024;67(3):2129–51.
44. Ma CY, He N, Zhao YY, Xia DD, Wei JF, Kang WY. Antimicrobial mechanism of hydroquinone. Appl Biochem Biotechnol. 2019;189:1291–303.

45. Long GQ, Li XM, Wang DD, Bao TRG, Yang YC, Zheng YY, et al. Prenylated flavonoids and derivatives isolated from the root barks of *Sophora flavescens* as potent antibacterial agents against *Staphylococcus aureus*. Ind Crop Prod. 2022;189:115834.
46. Liu ZY, Zhou QY, Xue JJ, Cui MH, Xu L, Fang TQ, et al. Recent discoveries of propyl gallate restore the antibacterial effect of tigecycline against tet (X4)-positive *Escherichia coli*. Biochem Pharmacol. 2025;231:116638.
47. Chang S, Li Y, Huang X, He N, Wang M, Wang J, et al. Bioactivity-based molecular networking-guided isolation of epicolidines A-C from the endophytic fungus *Epicoccum* sp. 1–042. J Nat Prod. 2024;87(6):1582–90.

Publisher's Note